19th Australasian Fluid Mechanics Conference
Melbourne, Australia
8-11 December 2014

19th Australasian Fluid Mechanics Conference: Flow-induced Structural Instabilities via Spring-Mounted Lifting Flexible Plates in a Uniform Flow for Energy Harvesting

R. M. Howell[1] **and A. D. Lucey**[1]

[1]Fluid Dynamics Research Group, Department of Mechanical Engineering,
Curtin University of Technology, GPO Box U1987, Perth, Western Australia 6845

Abstract

In this paper, two mounting systems are studied and compared. The first is a new system in fluid-structure interaction (FSI) wherein a cantilevered thin flexible plate is aligned with a uniform flow with the upstream end of the plate attached to a spring-mass system: this allows the entire system to oscillate in a direction perpendicular to that of the flow as a result of the mounting's dynamic interaction with the flow-induced oscillations, or flutter, of the flexible plate; we compare this system to one where the upstream end is hinged with a rotational spring at the mount. While the first system is a fundamental problem in FSI, the study of this variation on classical plate flutter is also motivated by its potential as an energy-harvesting system in which the reciprocating motion of the support system would be tapped for energy production.

In this paper we formulate and deploy a hybrid of theoretical and computational models for the fluid-structure systems and map out their linear stability characteristics. The computational model detailed is a fully-implicit solution that is very robust to spatial and temporal discretisation. Compared to a fixed cantilever, the introduction of the dynamic support in both systems is shown to yield lower flutter-onset flow speeds and for the spring-mounted cantilever a reduction of the order of the mode that yields the critical flow speed; these effects would be desirable for energy harvesting applications.

Introduction

Recent practical motivation for the renewed study of cantilevered flexible plates in axial flow - a problem first studied in the modern era by [4] - is the potential to use flow-induced oscillations, or flutter, of the flexible plate to capture kinetic energy from the mean flow above a critical flow speed, examples of these recent studies being [8; 7] wherein the latter reference utilises an articulated beam. We therefore conceive the spring-mounted cantilever system illustrated in figure 1(a) wherein the flow-induced oscillations of the flexible plate drive vertical oscillatory motion of a mass-spring support system having its own dynamics that can clearly be tuned. As shown in the figure, the extraction of power can be modelled by the inclusion of linear damping at the support. We compare this *shear force* device with that of a *bending moment* device that is illustrated in figure 1(b) which comprises a hinged-free plate with a rotational spring. In this paper we therefore develop a theoretical and computational model of the two-dimensional systems and map out the dynamics of the remaining parameter space that we find has the usual non-dimensional control parameters, mass ratio $\bar{L}$ and flow speed $\bar{U}$, for a fixed cantilever, in addition to which there are the natural frequencies of the spring-mass support systems, $\bar{\omega}_s$ and $\bar{\Omega}_s$ for the translational and rotational systems respectively, where the subscript 's' throughout this paper signifies a spring-mount property.

To this end, the method of [2] that mixed numerical simulation with eigenvalue analysis is built upon. Thus, ideal two-dimensional flow is assumed wherein the rotationality of the boundary-layers is modelled by vortex elements on the solid-fluid interface and the imposition of the Kutta condition at the plate's trailing edge. The Euler-Bernoulli beam model is used for the structural dynamics. The latter is appropriate because it is our overall objective to design and optimise an energy-harvesting system that operates for low-amplitude deformations - to reduce material fatigue effects - of the flexible plate by tuning the support system such that the available wind speed coincides with the modified critical speed of flutter onset of the flexible plate. The results presented in this paper demonstrate that this strategy is practicable.

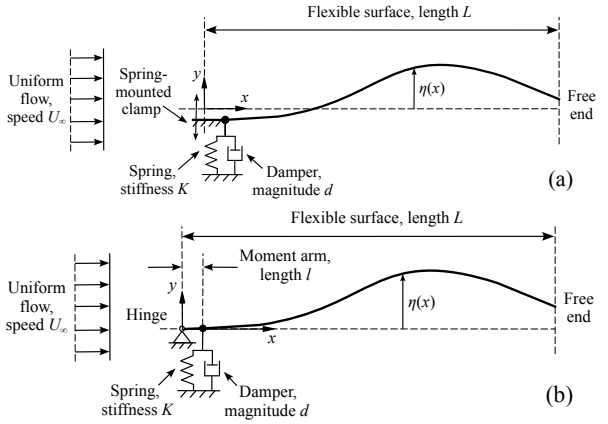

Figure 1: The fluid-structure systems under consideration: (a) spring-mounted cantilever; (b) hinged-free plate with rotational spring at the leading edge.

Theoretical & Computational Modelling

The essential modelling is described in detail in [2] wherein the system of figure 1(a) was mounted rigidly and symmetrically within a channel with its walls located at $y = \pm H$; the present system is obtained by letting $H \to \infty$. For the present paper, we also neglect the effects of the wake that were modelled in the precursor paper. The system of figure 1(b) is essentially the same as the system described in [2] except for the application of a hinged condition at the leading edge of the plate instead of a clamp and therefore this section is given to description of the system in figure 1 (a) which is an extension of our work detailed in [3].

Simply supported free plates where the support can move vertically and actuate the system have been analysed in studies of insect flight and base-excited, fluid-conveying flexible tubes, for example see [5] and [1] respectively, and constrain that the leading edge must follow the actuating force. In our study as well as applying an actuating force due to the reaction of the spring, we allow that the motion of the leading edge can also be actuated by the motion of the flexible plate; these constraints are applied through the inclusion of a shear-force balance condition at the leading edge that transmits the shear force that drives the vertical motion of the mounting system whilst also enforc-

ing that neither free nor controlled rotation of the plate about its leading edge is permitted; this means that the support mechanism can provide, without deformation, any level of moment reaction to the flexible plate at its upstream end.

Referring to [6] the shear force in the flexible plate at the leading edge is calculated through the following equation of motion for $\eta_s(t)$,

$$B\frac{\partial^3\eta_s}{\partial x^3} = -\left((\rho h)_s^*\frac{\partial^2\eta_s}{\partial t^2} + K_s^*\eta_s\right), \tag{1}$$

and where $\eta(x,t)$ is the flexible-plate vertical-displacement field and B, ρ and h are respectively the flexural rigidity, material density and thickness of the plate; K_s is the mount spring-stiffness. The superscript * denotes units of force per-metre width of the infinitely-wide mount since this equation represents a force balance: for example $K_s^* = \int_s K_s \mathrm{d}x$. It can be seen that the shear condition joins two separate systems: a vertically oscillating flat plate with a vertically oscillating flexible plate.

This condition is used to solve for the second boundary condition mass point η_{-2}; to solve for the first boundary condition mass point η_{-1} we enforce that the clamp extension is flat by setting that the first mass point in the system is horizontally in line with the clamp; we therefore have the following equations for the first boundary condition mass point

$$\eta_{-1} = \eta_1 \quad \text{and} \quad \dot{\eta}_{-1} = \dot{\eta}_1. \tag{2a, b}$$

The hinged-free plate does not require the shear condition in equation (1); the dummy node solutions for a hinged end for which boundary conditions of zero displacement and zero bending-moment are enforced are

$$\eta_{-1} = 0 \quad \text{and} \quad \eta_{-2} = -\eta_1. \tag{3a, b}$$

We now summarise how the conditions in equations (1), (2) and (3) for the spring-mass systems are readily incorporated in the model. The flow field is found using a linearised boundary-element method (BEM) with quantity N first-order vortex panels on the flexible plate of length L - panel length for a uniform discretisation is defined as $\delta x = L/N$. Vortex singularities are used because of the discontinuity of tangential fluid velocity across the plate that makes it a lifting surface; the distributed lift drives the motion of the flexible plate. The singularity strengths are determined by enforcing the no-flux boundary condition at every panel control point and continuity of the distributed vorticity between adjacent panels in the discretisation. In addition the boundary condition of zero vorticity at the plate's trailing edge is applied, thus enforcing the standard Kutta condition of zero pressure difference at the trailing edge for linear displacements.

The unsteady Bernoulli equation is utilized to determine the pressure distribution on the flexible plate. The transmural pressure is then used as the forcing term in the one-dimensional thin flexible-plate equation couched in finite-difference form. The motions of the plate and the fluid flow are fully coupled through deflection, vertical velocity and acceleration of the two media at their interface. This allows the following single system (matrix) equation to be written

$$\begin{aligned}\rho h[\mathbf{I}]\{\ddot{\eta}\} + B[\mathbf{D_4}]\{\eta\} + \{K\}[\mathbf{I}]\{\eta\} &= 2\rho_f U_\infty^2\left[\mathbf{B_1^+}\right]\{\eta\} \\ + \rho_f U_\infty\left[\mathbf{B_1^-}\right]\{\dot{\eta}\} + \rho_f U_\infty\left[\mathbf{B_2^+}\right]\{\dot{\eta}\} &= \rho_f[\mathbf{B_2}]\{\ddot{\eta}\}.\end{aligned} \tag{4}$$

The pressure perturbation that drives the plate motion appears on the right-hand side, where ρ_f and U_∞ are the fluid density and free-stream velocity respectively and $[\mathbf{B}]$ are matrices of singularity influence coefficients: the $[\mathbf{B}]$ matrices marked with a $+$ or $-$ have been suitably rearranged to have the equations in terms of η instead of linearised panel slope θ and averaged values of η. The fluid pressure terms that depend on plate displacement, velocity and acceleration in equation (4) can be interpreted as the hydrodynamic stiffness, damping (two terms) and inertia respectively. The plate pressure terms appear on the left-hand side: $[\mathbf{D_4}]$ is a fourth-order spatial-differentiation matrix and $[\mathbf{I}]$ is the identity matrix; note that the vector $\{K\}$ only has a value at the first mass point. The boundary conditions of equations (1), (2) and (3) are applied where necessary in the leading-edge values of $[\mathbf{D_4}]$, $[\mathbf{B^+}]$ and $[\mathbf{B^-}]$.

We take two approaches to the solution of equation (4) rearranged as the system

$$\{\ddot{\eta}\} = [\mathbf{E}]\{\dot{\eta}\} + [\mathbf{F}]\{\eta\}, \tag{5}$$

where $[\mathbf{E}]$ and $[\mathbf{F}]$ are readily inferred from equation (4). In the first approach we reduce the second-order ordinary differential equation in η to first-order using the state-space variables $w_1(t) = \eta(t)$, $w_2(t) = \dot{\eta}(t) = \dot{w}_1(t)$ that therefore allows $\ddot{\eta}(t) = \dot{w}_2(t)$. Rearranging in companion-matrix form, single-frequency time-dependent response is assumed at ω which is a complex eigenvalue of the companion-form. Positive ω_I and ω_R respectively represent the oscillatory and amplifying parts of the response. As the flexible plate is discretised into N mass points we therefore extract $2N$ system eigenmodes.

Alternatively, we perform a time-discretisation of the system and then numerically time-step the equation using a fully-implicit method to determine the system response to an applied form of initial perturbation that we detailed in [3]. In doing so we are able to study transient behaviour and reveal localised flow-structure dynamics that when summed contribute to the system response. The latter method is very robust to spatial and temporal discretisation and requires only a single or double iteration per time step to converge. It is noted that this method is only applicable to linear deflections of a linearised or non-linear system.

Results

Our results are presented in non-dimensional form using the scheme detailed in [2] whereby reference time and length are

$$t_r = (\rho h)^{\frac{5}{2}}/(\rho_f^2 B^{\frac{1}{2}}) \ \text{ and } \ L_r = \rho h/\rho_f, \tag{6a, b}$$

and therefore non-dimensional velocity, time and plate oscillation frequency are calculated as

$$\bar{U} = U_\infty t_r/L_r, \ \bar{t} = t/t_r \ \text{ and } \ \bar{\omega} = \omega t_r. \tag{7a, b, c}$$

The non-dimensional streamwise coordinate and length (or mass ratio) of the flexible plate are defined by

$$\bar{x} = x/L \ \text{ and } \ \bar{L} = L/L_r. \tag{8a, b}$$

This scheme permits $\bar{U}$ and $\bar{L}$ to be interpreted respectively as the physical flow speed and plate length for given fluid and plate properties. To characterise the mounting systems, we non-dimensionalise $\bar{\omega}_s$ and $\bar{\Omega}_s$ so that

$$\bar{\omega}_s = (K_s^*/M_T^*)^{\frac{1}{2}} t_r \ \text{ and } \ \bar{\Omega}_s = (\kappa_s/I_T)^{\frac{1}{2}} t_r, \tag{9a, b}$$

where $M_T = \rho h L$ is the total plate mass, I_T is the total moment of inertia of the plate about the hinge and $\kappa = K_s^* l^2$ is the rotational spring stiffness, where l is the moment arm shown in figure 1b. In summary, we find that the critical velocity and frequency of the system $\bar{U}_c$ and $\bar{\omega}_c$ take the functional dependence on the system's control parameters $f(\bar{L}, \bar{\omega}_s$ or $\bar{\Omega}_s)$.

With respect to the system energy equation, the introduction of a spring-mount into our numerical simulations causes important changes in the energy evolution of the system that are reflected in a modification to the standard formulation. Adapting the derivation of [2], the plate energy equation is generated

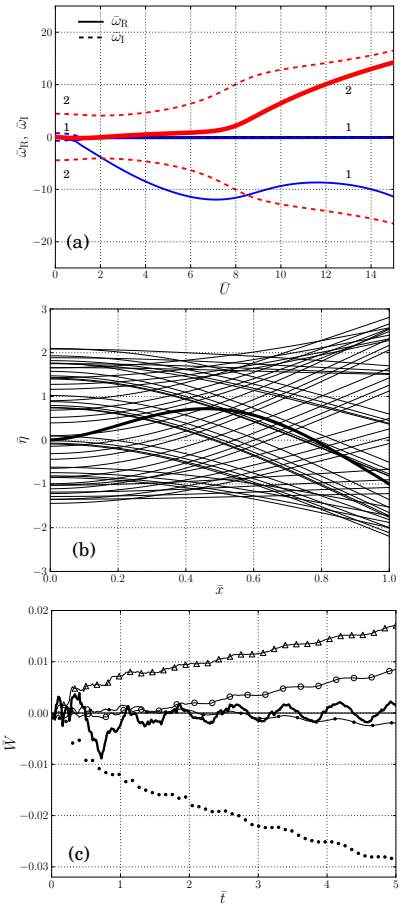

Figure 2: System dynamics for $\bar{L} = 1$ with $\bar{\omega}_s = 1$: (a) Variation of numbered eigenvalues with flow speed (oscillatory and growth/decay parts represented by broken and full lines respectively) with the real part of Mode 2 that becomes unstable highlighted through a thicker line type, (b) time-sequence of instantaneous plate position (the thick line being the initial deflection with early oscillations removed), (c) time series of cumulative energy transferred from flow to plate in –△– first, –○– second, –●– third, and ⋯ fourth quarters of the plate while —— (thick) is the total of these; (b) and (c) at $\bar{U}_c = 2.2$.

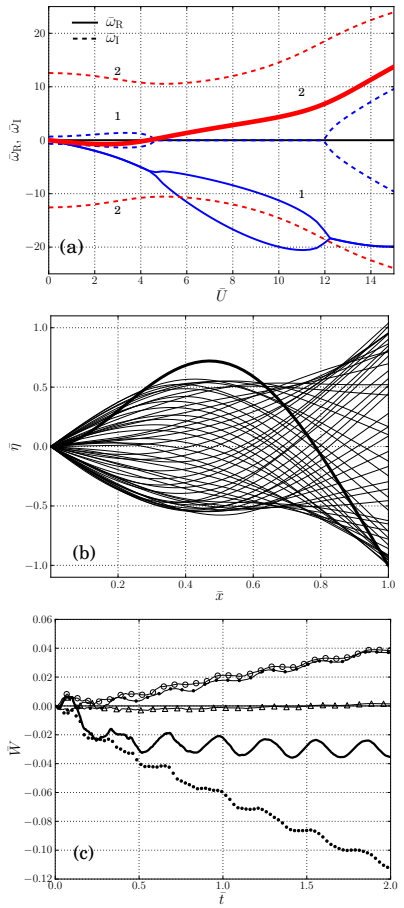

Figure 3: System dynamics for $\bar{L} = 1$ with $\bar{\Omega}_s = 1$: (b) and (c) at $\bar{U}_c = 4.3$; Other descriptions as figure 2.

by multiplying the continuous version of equation (4) by $\dot{\eta}$ and integrating along the length of the flexible surface so that

$$\frac{\partial}{\partial t}\left(\underbrace{\frac{1}{2}\rho h\int_0^L \dot{\eta}^2 \mathrm{d}x}_{E_K} + \underbrace{\frac{1}{2}B\int_0^L \eta_{,xx}^2 \mathrm{d}x + \frac{1}{2}K_s^*\eta_s^2}_{E_S}\right) = \int_0^L (-\delta p)\,\dot{\eta}\,\mathrm{d}x + B\eta_{s,xxx}\dot{\eta}_s. \tag{10}$$

The kinetic and strain energies of the plate are E_K and E_S respectively. Equation (10) shows that the plate energy either grows or decays in time depending upon the rate of work done by the pressure loading, $(-\delta p)$. It is clear that for neutrally stable low-amplitude oscillations at the critical flutter speed the left-hand side of equation (10) is zero (no energy growth) and thus is exactly equal to the energy-transfer rate - $\dot{W}$, the first term on the right-hand side - from the flow to the flexible plate via the pressure field over the entire flexible plate plus the second term on the right-hand side.

This latter term is the work done on the spring mount to enforce that the clamp stays horizontal; $\eta_{s,xxx}$ is calculated from the boundary condition in equation (1). Clearly the extra term means that (some) energy is wasted when the support is constrained to move vertically as a clamp, whereas when there is a torsional spring on a hinged support none is wasted as this term is zero.

The non-dimensional form of $\dot{W}$ we plot in our results is $\bar{W}(t_p)$ that represents the sum of pressure work done up to time t_p - therefore corresponding to the current value of total plate energy $E_T = E_S + E_K$ - divided by the initial strain energy of the plate deformed in the second eigenmode.

Figure 2 shows the results at $\bar{L} = 1$ with $\bar{\omega}_s = 1$. Figure 2a shows the variation of system eigenvalues with applied flow speed. The broken lines denote the oscillatory (imaginary) part of the eigenvalue, ω_I, while the solid lines show the associated growth/decay (real) part of the eigenvalue, ω_R. The modes are numbered in the plots following their order of increasing frequency at zero flow speed. Instability sets in at the lowest flow speed (the critical flow speed, $\bar{U}_c$) for which ω_R becomes positive, *i.e.* that at which the ω_R locus crosses the horizontal axis to move into the upper positive quadrant of the plot. In figure 2a it is seen that single-mode flutter of the second system mode - highlighted by a thicker line type - is the critical instability at a non-dimensional flow speed $\bar{U} = \bar{U}_c = 2.2$.

This instability has a strong mode 1 content that can be seen in the critical mode shape at this flow speed, figure 2b showing a numerical simulation of the critical mode evolution. The simulation was started by releasing the plate from an applied deformation - the thick black line - in the shape of the second *in-vacuo* mode. The critical mode then evolves from the initial excitation.

The plate-energy record for the simulation of figure 2b is shown in figure 2c: the thick line represents the total energy transferred from the flow to the plate exactly at the critical flow

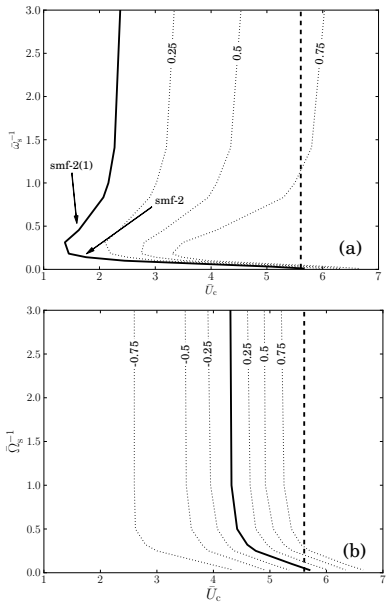

Figure 4: System dynamics for $\bar{L} = 1$: Plots of $\bar{\omega}_s^{-1}$ against $\bar{U}_c$ for (a) spring-mounted cantilever, and (b) hinged-free plate with rotational spring at leading edge; dashed lines denote $\bar{U}_c$ for the fixed cantilever case from [2]; dotted lines are $\bar{\omega}_R$ values and are therefore contours of instability intensity.

speed where neutral stability occurs, while the other four lines show the contributions to this total from each of the four quarters of the plate. After transients due to mode adjustment have died away, the time-averaged value of the total energy is constant. However, it is also seen that the energy exchanges between plate and flow are spatially dependent. Figure 2c shows that the destabilising work done by and on the fluid is in the first quarter of the plate where the greatest energy transfer is occurring in the system.

In comparison, the hinged-free system for $\bar{\Omega}_s = 1$ shown in figure 3 is very similar to the equivalent fixed-cantilever result in [2] for $\bar{H} = 1$ (for which the channel walls were shown to exert negligible effect): figure 3b shows that the critical mode shape loses most of its first-order mode content and becomes more second-mode dominated, the reason for this being the absence of the stronger real component of the first mode just below the x-axis, as shown in figure 3a. Also, figure 3c shows that the location of the destabilising fluid-work done on the plate moves to the third quarter of the plate.

Figure 4 shows how the critical speeds of instability onset vary with the spring-mounting characterised by $\bar{\omega}_s$ and $\bar{\Omega}_s$ for $\bar{L} = 1$. The vertical dashed lines show $\bar{U}_c$ values for the fixed cantilever case. We remark that the detailed results of figures 2 and 3 appear as the data point for $\bar{\omega}_s^{-1} = \bar{\Omega}_s^{-1} = 1$ in figures 4a and 4b respectively. Figure 4 shows that the introduction of a spring-mounting destabilises the system - critical flow speeds are lower - than for the fixed cantilever. The onset flow speeds are seen to approach those of the fixed cantilever as $\bar{\omega}_s$ or $\bar{\Omega}_s$ is increased ($\bar{\omega}_s^{-1}$ or $\bar{\Omega}_s^{-1}$ is decreased) although a very small numerical difference between the new mobile and previous [2] fixed cantilever models appears: this is most probably due to ill-conditioning of the system stiffness matrix as the value of the spring-support coefficient is made extremely large.

In both cases the system is nearly always destabilised by single-mode flutter of mode 2 as typified in [2]: however, in figure 4a we note that at $\bar{\omega}_s^{-1} = 0.25$ there is a change in the instability for the spring-mounted cantilever as the critical mode content switches to be mode 1 dominated with its different route to instability as seen in figure 2. The frequencies of the critical mode - not shown here - approach those of the fixed system as the spring stiffness is increased. The introduction of a spring-mounting decreases the oscillation frequencies of the critical mode in proportion with the reduction in critical velocity as compared with the fixed-cantilever for both cases.

Comparing instability intensity between the systems, we see that although the spring-mounted cantilever has a lower critical velocity for most values of mount spring-stiffness, the hinged-free system has a more severe instability for those values. This means that the hinged-free system is more generally practicable for energy-harvesting applications as it does not require a specialised spring-mount set-up to take advantage of a smaller band of parameters where the system is sufficiently unstable for energy-harvesting purposes.

Conclusions

We have developed models for predicting the two-dimensional linear-stability characteristics of spring-mounted flexible plate in a uniform flow. The basic stability characteristics of the system have been investigated for cases that, for a rigid mounting, would succumb to single-mode flutter. It has been shown that the introduction of a spring-mounting is destabilising in that it leads to lower values of $\bar{U}_c$. As the natural frequency of the mounting system is reduced, both systems asymptote to a fixed value of $\bar{U}_c$ associated with rigid-body motion: in effect the flexible plate becomes very stiff as compared with the mounting system. For the spring-mounted cantilever a value is reached for which $\bar{U}_c$ is a local minimum: this minimum exists because the critical-mode content evolves from one of a higher to a lower order that can then become more stable with further decreases to the mounting stiffness. These stability findings augur well for the introduction of means to extract power from the reciprocating motion - linear or rotational - of the support. The present methods could then be used to determine optimal system parameters for energy harvesting.

References

[1] Chang, G. H. and Modarres-Sadeghi, Y., Flow-induced oscillations of a cantilevered pipe conveying fluid with base excitation, *Journal of Sound and Vibration*, **333**, 2014, 4265–4280.

[2] Howell, R. M., Lucey, A. D., Carpenter, P. W. and Pitman, M. W., Interaction between a cantilevered-free flexible plate and ideal flow, *Journal of Fluids and Structures*, **25**, 2009, 544–566.

[3] Howell, R. M., Lucey, A. D. and Kapor, J. S., Stability of a spring-mounted cantilevered-free flexible plate in a uniform flow, in *Proceedings 18th Australasian Fluid Mechanics Conference*, Launceston, Australia, 2012.

[4] Kornecki, A., Dowell, E. H. and O'Brien, J., On the aeroelastic instability of two-dimensional panels in uniform incompressible flow, *Journal of Sound and Vibration*, **47**, 1976, 163–178.

[5] Manela, A., Vibration and sound of an elastic wing actuated at its leading edge, *Journal of Sound and Vibration*, **331**, 2012, 638–650.

[6] Rao, S. S., *Mechanical Vibrations*, Pearson, Upper Saddle River, NJ, 2011, 5 edition.

[7] Singh, K., Michelin, S. and de Langre, E., Energy harvesting from axial fluid-elastic instabilities of a cylinder, *Journal of Fluids and Structures*, **30**, 2012, 159–172.

[8] Tang, L., Païdoussis, M. P. and Jiang, J., Cantilevered flexible plates in axial flow: Energy transfer and the concept of flutter mill, *Journal of Sound and Vibration*, **326**, 2009, 263–276.